Miniature Fluidic Microtissue Culturing Device for Rapid Biological Detection

Patrick M. Misun, Andreas Hierlemann and Olivier Frey

Abstract Microfluidics is becoming a technology of growing interest to build miniature culturing systems, capable of mimicking tissue functions and multi-tissue interactions in so-called "body-on-a-chip" applications while featuring integrated readout functionalities. This chapter presents a highly versatile, modular and scalable analytical platform technology, which combines microfluidic hanging-drop networks with multi-analyte biosensors for in situ monitoring of the metabolism of 3D microtissues. The microfluidic platform is based on the hanging-drop network technology, which has been designed for formation, cultivation, and analysis of fluidically interconnected organotypic spherical 3D microtissues that can be obtained from various different cell types. The sensor modules were designed as small glass plug-ins, which allow for convenient functionalization and calibration of the sensors and do not interfere with the microfluidic functions. They were placed in the ceiling substrate, from which the hanging drops that host the spheroid cultures were suspended. The detection of secreted lactate of single microtissue spheroids will be presented. Further, we will demonstrate that it is possible to monitor microtissue lactate secretion and glucose consumption in parallel.

1 Combining Microfluidic Systems, 3D Microtissue Culturing and Biosensor Systems

Microfluidics technology offers engineering of a variety of new methods and platforms for culturing and analyzing human cells and tissue structures [14, 32]. Tissue models that reproduce in vivo conditions as closely as possible are important for

P.M. Misun · A. Hierlemann · O. Frey
Bio Engineering Laboratory, Department of Biosystems Science and Engineering, ETH Zurich, Mattenstrasse 26, 4058 Basel, Switzerland

O. Frey (✉)
InSphero AG, Wagistrasse 27, 8952 Schlieren, Switzerland
e-mail: olivier.frey@insphero.com

S.-H. Oh et al. (eds.), *Miniature Fluidic Devices for Rapid Biological Detection*, Integrated Analytical Systems, https://doi.org/10.1007/978-3-319-64747-0_8

understanding organ-specific cell behavior for investigating diseases and for finding new compounds and therapies in the drug discovery process [16, 28, 42, 45].

Testing new compounds, and studying cellular responses and metabolism in preclinical trials by using monolayer cell systems in standard well plates has the advantage that one can rely on established techniques and laboratory equipment for cell handling and imaging at high throughput. Conventional 2D cell cultures, however, have limitations in mimicking functional living tissue, as the native microenvironment including cell-to-cell interaction, mechanical cues, and spatiotemporal biochemical gradients is not present [2, 4, 31]. Advancing cell culturing systems that potentially overcome these limitations is of great interest and gains more and more momentum in pharmaceutical industry and basic research [8].

Major efforts are made in developing 3D cell culture models that better reproduce the physiological tissue morphology and properties. A wide spectrum of 3D cell culture methods and materials are currently being developed [23, 33, 54]. Spheroids, for example, are a popular choice as scaffold-free 3D microtissues. Different types of spheroids can be formed through self-aggregation in hanging drops to mimic functional tissue of several organs, while they retain their specific characteristics and functions during an extended period of time [6, 25, 29, 38, 47, 56].

A second aspect of advanced culture systems is the integration of continuous perfusion capabilities and the possibility to integrate fluid-dynamic and mechano-dynamic cues to even better mimic the in vivo environment [60]. Perfusion, for example, can be modulated to provide tissue-specific environmental conditions [15, 46] and to simulate shear forces that are present at the interface of tissues in their fluidic environments [5, 35, 57]. Flexible substrates can be implemented to mimic the oscillatory mechanical stress in lung alveoli [26, 51]. Interconnected fluidic networks, finally, offer the possibility to combine different cell cultures or tissue types to realize “body-on-a-chip” configurations [27, 30, 36, 50, 52, 58, 61].

The third aspect relates to established analysis methods, which predominantly have been designed to meet the requirements of 2D cell cultures. Analysis methods and assays have to be adapted for 3D cell cultures and the corresponding platforms in order to fully capitalize on the advantages of 3D cell culture formats. Most metabolic processes are dynamic and occur within a few minutes. Thus, studying time-resolved responses of cell cultures upon environmental changes or upon defined compound dosage often requires continuous readout in order not to miss the occurrence of important events [34]. In well-based approaches, liquid handling is discrete, which entails a large risk that one may miss events. Moreover, conventional cell assays usually include relatively large sample volumes. Frequent sampling of the cell culture medium interrupts and disturbs the overall culturing process, increases the risk of contaminations, and may entail extensive dilution of important markers or metabolites in the process through the accompanying addition of new medium. As cell-to-medium volume ratios are comparably low, frequent sampling also entails the risk that metabolite concentrations fall below the limit of detection.

Microfluidics, in contrast, offer precise flow handling of small liquid volumes and accurate control over microenvironmental parameters that are important in

analytical cell culture devices [14]. Additionally, microfabrication techniques offer multiplexing capabilities, and allow for straightforward integration of novel modules, such as pumping systems, actuators, and microsensors [12, 41]. Microsensor technologies have been developed since decades for a variety of applications. Their miniature size and versatile features, their high sensitivity and low detection limits enable monitoring of various analytes in cell and tissue culture setups at high temporal and spatial resolution.

Many multi-sensor systems were designed as probes, mostly comprising of electrochemical biosensors, and have been applied to conventional cell culture assays to monitor microphysiological conditions over time [13, 22, 24, 37]. Miniaturized versions have been used as scanning probes to monitor the glucose and lactate metabolism of single cells [10, 44]. Flow-through-type sensor systems have been devised to analyze cell culture conditions and metabolites in liquid samples downstream of cell cultures [1, 7, 11, 18, 40, 43, 49, 53]. Silicon-based sensor chips for multi-parameter online monitoring have been mounted in a perfused cell culture unit [9], and multiple sensing electrodes were directly incorporated into transparent microfluidic systems to measure glucose consumption of single cardiac cells [20], lactate production of various cell types [21] and for monitoring cancer cell metabolism in combination with an optical readout [59].

The combination and integration of microfluidics and microsensors with cell culturing units poses several challenges. Fabrication methods of the different components need to be compatible, and all target features and functions need to be preserved over the duration of an experiment; cell cultures need to stay viable and functional, microfluidic handling needs to be robust and precise, sensors need to meet the detection specifications including sensitivity and selectivity. The use of 3D cell cultures in microfluidic setups and the realization of multi-tissue configurations render this integration even more complex.

This chapter describes a technological approach to combine 3D microtissue spheroids, used as a 3D cell culture model, with a microfluidic perfusion system and the integration of biosensor-based online monitoring. For further details also refer to [39].

2 Microfluidic Hanging-Drop Networks

Scaffold-free 3D spherical microtissues can be formed by seeding a defined number of cells into hanging drops of a specific culture medium. Cells sediment by gravity force, self-aggregate and form a spherical microtissue at the liquid–air interface [29]. The liquid–air interface is an important component, as it prevents cell adhesion and promotes subsequent scaffold-free cell culturing and tissue maturation. A next step is to connect the hanging drops to each other by using miniature channels, which the yields hanging-drop networks (HDNs). HDNs combine isolated hanging drops into fully interconnected networks of hanging drops and enable controlled liquid flow between the hanging drops [17]. Adding perfusion substantially expands the

experimental options for 3D spherical microtissues by adding the features of continuous medium exchange, application of compound-dosage protocols, and the biochemical interaction of different microtissues through the liquid medium in multi-tissue or so-called "body-on-a-chip" setups.

2.1 Design

Hanging-drop networks are designed as completely open microfluidic systems at the bottom of an inverted, surface-patterned substrate. Figure 1a shows a basic five-drop-row configuration with a single fluidic inlet and a single fluidic outlet. The surface patterns guide the liquid by surface tension and capillary forces. Rim structures are used to distinguish wetted regions from dry regions and prevent the liquid from flowing over the whole surface in an uncontrolled way. The design of the rim structures defines, where drops are formed (Fig. 1b). Circular patterns induce the formation of hanging drops (cross-section 1), whereas narrow regions yield channel-like structures (cross-section 2). The dimensions have been optimized with regard to cell loading, drop and network stability, and perfusion characteristics [17]. Many different arrangements and configurations of hanging-drop networks can be realized through the variation of feature dimensions. An example is given in Fig. 1c depicting an array of four by four drops connected to a preceding

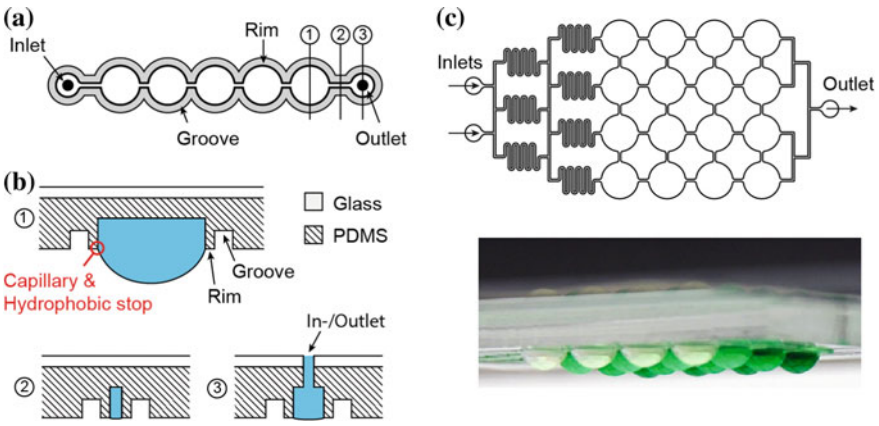

Fig. 1 Design of microfluidic hanging-drop networks. **a** A row of five interconnected hanging drops. Small rim structures confine the fluidic channels and drop structures. Hanging drops are formed at the circular regions interconnected through narrow channels. Inlet and outlet enable liquid perfusion. **b** Cross-sectional view through (1) hanging-drop structure, (2) channels, and (3) inlet and outlet position. The rim and groove act as phase guides. **c** Layout of a 4-by-4 hanging-drop network with integrated gradient generator. The photograph shows a side view of the chip during operation. Hanging drops of identical shapes are formed underneath the substrate. They were perfused with green food dye and a concentration gradient was formed across the array. Adapted from [17]

microfluidic gradient generator, which produces four different concentrations of a target compound by making use of integrated flow-splitting and -mixing structures.

Hanging-drop networks inherently fully exploit the benefits of the liquid–air interface, which include little or no cell adhesion and reduced compound adsorption on channel walls. Further, their open nature ensures gas exchange, prevents bubble formation and gives access to the liquid phase and the microtissues at every position in the network. The design is very versatile, so that a broad range of configurations can be designed.

2.2 Fabrication

The hanging-drop network structures are made of poly(dimethylsiloxane) (PDMS), casted from a microfabricated SU-8 mold (Fig. 2). The mold comprises of two layers of SU-8 that are successively spin-coated onto a 4 inch silicon wafer and processed using a standard photolithographic protocol (Fig. 2a–d). The two layers define the rim and the drop structures.

PDMS is prepared by mixing of elastomer and curing agent and pouring it onto the SU-8 mold (Fig. 2e). The cured ~3 mm thick PDMS replica is then peeled off the mold and cut into individual microfluidic chips (Fig. 2f). Holes are punched at predefined in- and outlet sites to enable fluidic connection via tubing. Microscopy

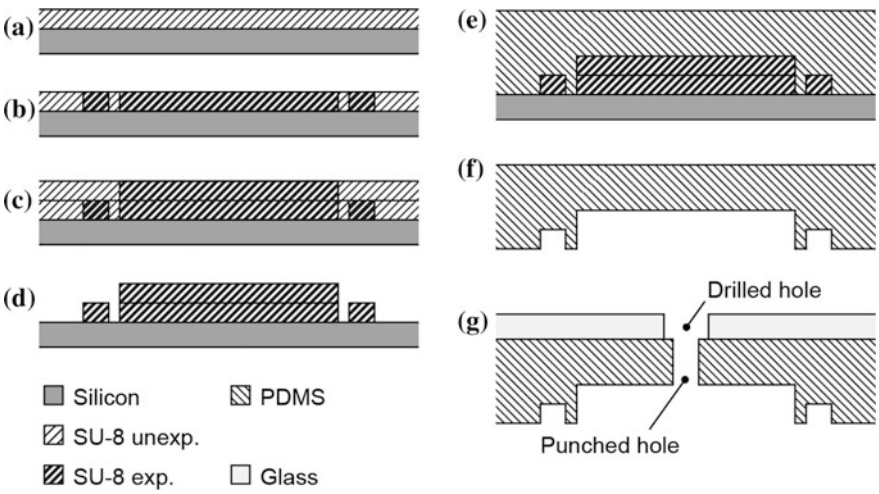

Fig. 2 Fabrication of the SU-8 mold and the microfluidic PDMS chip (schematic side view). **a** Silicon wafer with first layer of spin-coated SU-8 photoresist. **b** UV-exposed and cross-linked first SU-8 layer using a transparency mask. **c** Spin-coated and exposed second SU-8 layer. **d** Development of the non-cross-linked SU-8. **e** Casted and cured PDMS layer. **f** Cured PDMS layer removed from the SU-8 mold. **g** PDMS chip bonded to a glass substrate to make the chip more stable

slides are prepared with liquid access holes, and the PDMS chips are bonded to these slides after oxygen plasma surface activation. The glass slide improves planarity and mechanical stability of the system (Fig. 2g). The chips are placed in a custom-made chip holder and connected to conventional pumps via tubing.

3 Biosensor Integration

The biosensors are integrated into the hanging-drop networks in a modular approach. The final device consists of two parts: (i) the microfluidic PDMS chip and (ii) the small glass plug-ins featuring the biosensor electrodes (Fig. 3a). In this version, the hanging-drop network consisted of eight drops, arranged in two rows of four drops with three inlets and one outlet. The medium can be guided in parallel through the microfluidic structures allowing, for example, two different experimental conditions to be tested simultaneously.

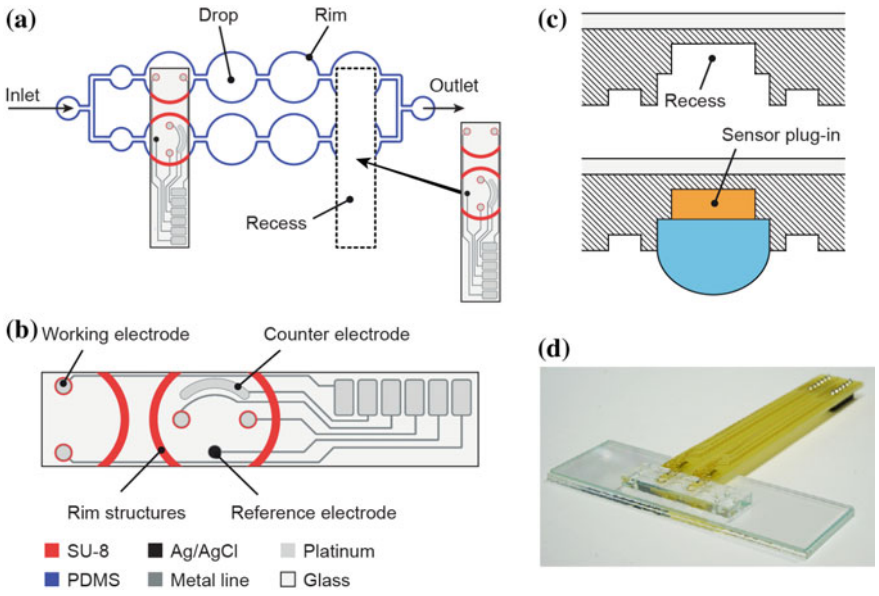

Fig. 3 Design and assembly of the hanging-drop-biosensor device. **a** Schematics of a 2-by-4 hanging-drop network showing the position and layout of the sensor plug-ins. The device consists of a microfluidic PDMS chip and two sensor glass plug-ins, which are inserted into a small recess. The PDMS rim (blue) and the SU-8 rim in the sensor plug-in (red) are complementary and close the fluidic network. **b** Layout of the sensor glass plug-in featuring four platinum working electrodes, one Ag/AgCl reference and a counter electrode. **c** Schematic cross-sectional view through a drop structure. The sensor is located at the ceiling of the hanging-drop structure. **d** Final assembly of the device. The sensor glass plug-in is connected to a PCB that facilitates the handling and provides an electric interface. Adapted from [39]

The sensor plug-ins extend over two drops and comprise six platinum electrodes and connection pads located on a glass substrate (Fig. 3b). For a seamless integration, the sensor units are inserted into a small rectangular recess in the PDMS chip, so that the electrodes are located at the ceiling of the hanging drop once the device is flipped upside down in the final assembly (Fig. 3c). The recess is produced with a third layer of the SU-8 mold.

Two circular working electrodes are integrated in each drop. Further, a counter electrode and an Ag/AgCl pseudo-reference electrode are integrated in one of the drops. SU-8 structures on the glass plug-in complete the rim patterns on the PDMS to obtain a leakage-free operation of the fluidic network. A completely assembled device is shown in Fig. 3d.

3.1 Fabrication

The sensor glass plug-ins are fabricated on a 4 inch glass wafer by using standard photolithography processes (Fig. 4). Thin-film platinum is sputtered on the glass and patterned in a lift-off process. A 500 nm thick Si_3N_4 passivation layer is then deposited onto the wafer using a plasma-enhanced chemical vapor deposition (PECVD) process. This passivation layer is re-opened at specified electrode and pad sites. Complementary rim structures and rings surrounding the electrodes on the sensor glass plug-in are fabricated by using SU-8 resist. The 20 µm SU-8 and the rim structures are fabricated with three layers of SU-8 according to the same procedure as described for the PDMS mold (Fig. 4f). At the end, the glass wafer is diced into single sensor glass plug-ins using a precision saw.

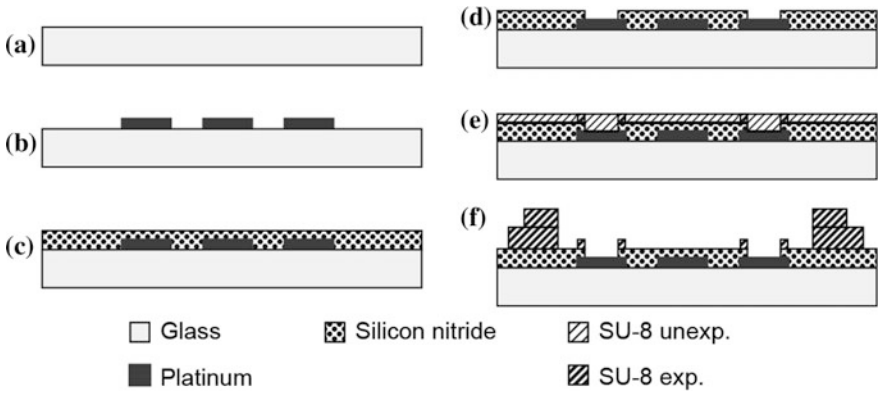

Fig. 4 Fabrication process of the sensor glass plug-in. **a**, **b** Platinum is deposited and patterned by using a lift-off process on a glass wafer by a photolithographic microfabrication processes. **c** A silicon nitride passivation layer is deposited onto the wafer surface for insulation. **d** The passivation layer is selectively removed at the electrode sites. **e** SU-8 is repeatedly spin-coated and UV exposed through a transparency mask in a three-layer process to structure the rim and liquid-phase guiding structures directly on the glass surface. **f** Final cross-section with developed SU-8

The individual glass plug-ins are glued onto a custom-made PCB, wire-bonded and packaged using epoxy glue. Connector pins were soldered to the PCB for electrical connections.

3.2 Assembly

For the final assembly of the device, sensor modules are inserted into the designated recesses on the microfluidic PDMS chip (Fig. 5a). Epoxy can be poured between the microscopy slide carrying the PDMS structures and the PCB to fix and stabilize the device.

Prior to each experiment, the assembled device is activated by an oxygen plasma treatment, while a thin PDMS mask with openings at the inlet, outlet, and all drop sites is used to cover all rim structures of the microfluidic hanging-drop device. This selective plasma treatment activates the inherently hydrophobic PDMS inside the circular drop structures and channel locations into a hydrophilic state. The covered rim structures remain hydrophobic and ensure that the liquid is confined.

The assembled device is clamped upside down onto a custom-made chip holder and placed into an OmniTray cultivation box, covered with a lid; wet cotton pads

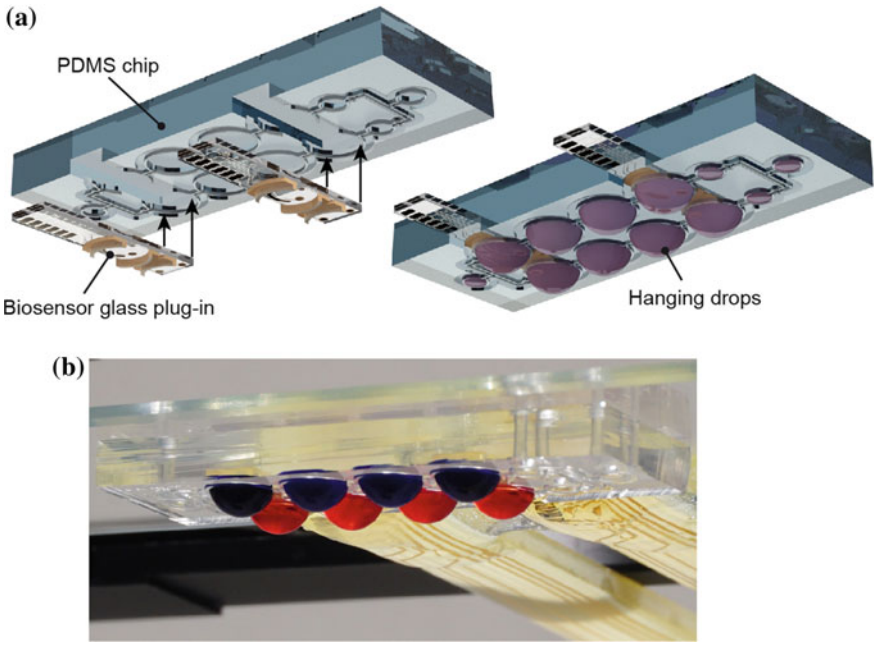

Fig. 5 Device assembly and operation. **a** Three-dimensional exploded view of the biosensor device. The sensor glass plug-ins are inserted into the recesses of the microfluidic PDMS chip. **b** Equally shaped hanging drops are formed directly underneath the patterned surface of the device. Two drop rows can be perfused with different media (indicated through different colors). Adapted from [39]

are included to provide additional humidity and to minimize evaporation. The sensor unit is electronically connected to an in-house fabricated CMOS-based multi-potentiostat for parallel current readout [48]. Precision syringe pumps are used for controlling the flow. The device is placed into an incubation box at controlled 37 °C, 5% CO_2, and 95% humidity for optimal culture conditions. Inlet tubing is connected to a heatable perfusion cannula so as to ensure constant temperature.

The device is loaded by pipetting 120 µl of liquid in one of the access holes, and eight hanging drops are formed underneath the circular regions (Fig. 5b). Each hanging drop comprises of a volume of ~10 µl, which includes the liquid in the cylindrical recess in the glass/PDMS substrate and the spherical drop fraction. The remaining liquid volume is in the channel and connection structures. The completely open PDMS chip architecture allows for easy access to the fluidic system and facilitates loading and harvesting of samples and spheroids during the experiments.

3.3 Electrode Preparation

An important advantage of the modular approach is that functionalization and calibration of the sensor can be carried out independently and before plugging the sensor unit into the microfluidic PDMS substrate.

All sensor units are initially sterilized with 70% ethanol, isopropanol and cleaned with oxygen plasma. The electrodes are tested by recording cyclic voltammograms in sulfuric acid solution. The reference electrode (RE) is coated with silver (Ag) through galvanostatic electrodeposition; the silver on the RE is subsequently partially transformed into AgCl. All four working electrodes (WEs) are coated with an m-polyphenylenediamine layer (mPPD) for rejection of potential electro-active interferant molecules. To improve the adhesion of the sensor hydrogel on the working electrodes, an additional (3-aminopropyl)triethoxysilane (APTES) layer is deposited through a vapor deposition process.

3.4 Biosensor Functionalization

A cross-section through the assembled microfluidic hanging-drop device and sensor unit is shown in Fig. 6a. The sensing electrodes allow for monitoring of the medium around the microtissues in the corresponding hanging drops. A simple drop-coating process is used to coat and functionalize the platinum working electrodes with a hydrogel containing glucose oxidase (GOx) or lactate oxidase (LOx). A schematic close-up of the hydrogel layer located directly on top of the sensing electrodes is shown in Fig. 6b. The enzymes catalyze an oxidation reaction of glucose or lactate that produces hydrogen peroxide, which, in turn, is

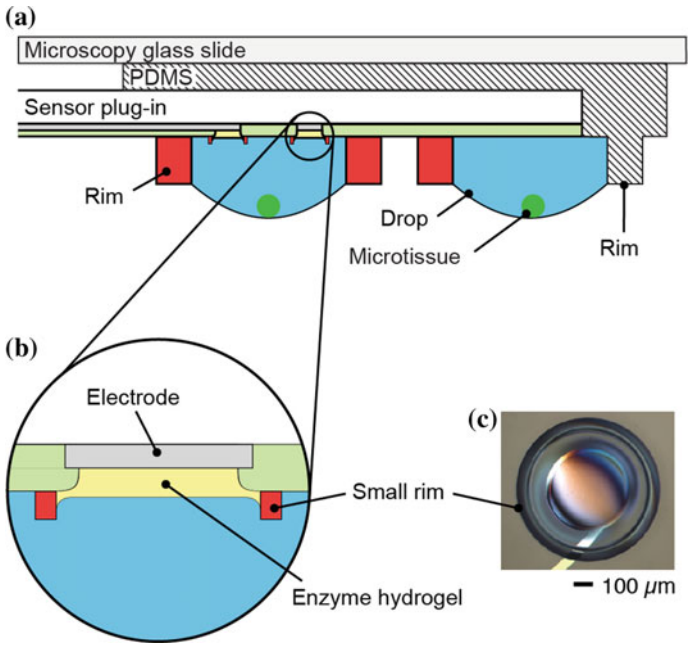

Fig. 6 Configuration and functionalization of the device. **a** Schematic cross-sectional view of the microfluidic biosensor device. Hanging drops form between the SU-8 rims on the glass plug-in and the microfluidic PDMS substrate. The biosensors are located at the ceilings of the hanging drops. **b** Close-up view showing the coating and functional layer of the electrodes. Enzymes (e.g. glucose oxidase or lactate oxidase) are immobilized in a hydrogel layer located directly on the electrodes. Analytes can be electrochemically detected on the electrode surface. **c** Photograph of a hydrogel-coated electrode showing the small SU-8 ring facilitating precise hydrogel deposition. Adapted from [39]

amperometrically detected on the Pt electrodes at a potential of 0.65 V versus Ag/AgCl. The current signal directly correlates with the analyte concentration of interest. A coated working electrode is shown in Fig. 6c. The enzyme-hydrogel is precisely located on the electrode area within the SU-8 ring structure. The ring structure facilitates the coating procedure and helps for achieving uniform hydrogel depositions on all electrodes.

The electrode coating is based on a co-cross-linking of the enzymes with bovine serum albumin (BSA) and glutaraldehyde (GA) [18]. Sub-microliter volumes of an aqueous solution containing one of the enzymes, BSA and GA are manually transferred onto the electrodes by touching the small rim structure surrounding the electrodes with a 2 µl pipette using appropriate tips. The hydrogel is formed directly on the electrodes by curing the solution at room temperature for at least 3 h before use.

3.5 Characterization of the Glucose and Lactate Biosensors

The biosensors were separately characterized through multiple calibration experiments "off-chip" and then after mounting into the microfluidic network "on-chip". Raw data of an off-chip calibration of three functionalized LOx working electrodes and one blank BSA electrode in a conventional 50 ml beaker is shown in Fig. 7a. After a 20 min settling at the beginning of the recording, lactate was successively added to the RPMI 1640 medium to increase the concentration. A specific current response to lactate was recorded. The limit of detection (LoD) was calculated to be 7.07 ± 2.73 µM (three times the background noise at the end of the settling time) for the lactate biosensor during an off-chip calibration at 37 °C under continuous stirring.

The biosensors showed reproducible characteristics with regard to linearity, sensitivity, and reproducibility for both, glucose and lactate (Fig. 7b). A linear relationship was observed for up to 2 mM glucose after coating of the electrode with a single GOx membrane ($R^2 > 0.99$). This sensor features a relatively high sensitivity of 322 ± 41 nA mM^{-1} mm^{-2}. The biosensor characteristics could be tuned by implementing additional layers on top of the enzyme membrane. Adding, for example, a diffusion-limiting BSA layer on top of the enzyme-hydrogel membrane increased the linear range up to 7 mM while decreasing the sensitivity to 88 nA mM^{-1} mm^{-2}. Implementing a catalase membrane on top of the enzyme membrane further increased the linear range to 11 mM. The respective sensitivity was determined to 30 nA mM^{-1} mm^{-2} [39]. The lactate sensor, based on a simple

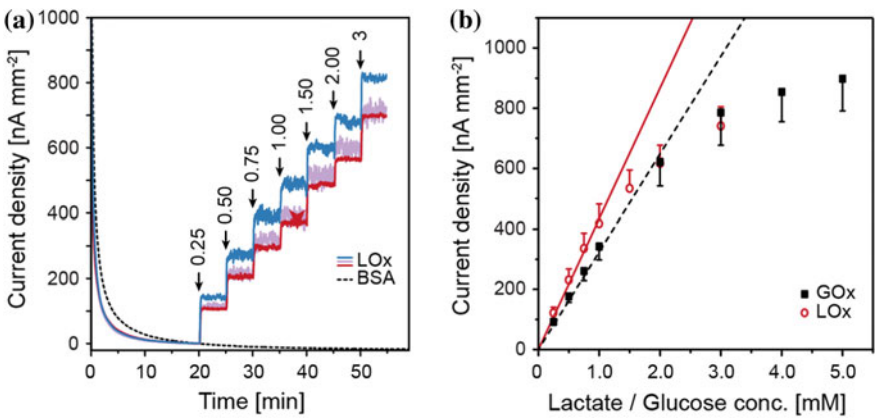

Fig. 7 Calibration and characterization of the glucose and lactate biosensors in RPMI 1640 medium at 37 °C. **a** Transient lactate current signals of three LOx- functionalized electrodes and one blank bovine serum albumin (BSA) electrode as a control. **b** Glucose and lactate calibration curves showing linear range and sensitivity of the biosensors. Adapted from [39]

LOx membrane coating on the electrodes, shows a linear response up to 1 mM and a sensitivity of 435 ± 66 nA mM^{-1} mm^{-2} in RPMI 1640 cell culture medium.

The biosensors were tested in the chip system in flow-through mode. Figure 8a displays simultaneously recorded raw signal traces of lactate biosensors and blank sensors during consecutive on-chip perfusion of 0, 0.25 and 0.50 mM lactate in PBS at a flow rate of 20 µl min^{-1} (10 µl min^{-1} in each row). The response of the biosensors was selective and reversible. The two lactate sensors showed slightly different sensitivities, which can be attributed to variations in the manual membrane deposition process. These variations demonstrate the importance of calibrations to be executed before any biological measurement. For this characterization experiment, several syringe pumps supplying the respective calibration solutions were connected to the device inlet via tubing. An artifact, which is caused by the change of the infusing syringe pump, indicates the change of the calibration solution. Tubing between syringes and microfluidic device produced a delayed sensor signal response. Based on the background noise, an LoD of 1.84 ± 0.34 µM was calculated for this calibration.

Figure 8b presents raw signal traces of a lactate and a glucose biosensor, combined in the same drop, in response to consecutive perfusion of PBS containing 1 mM glucose and 1 mM lactate at a constant flow rate of 5 µl min^{-1}. No sensor cross talk was observed in the continuous-flow mode.

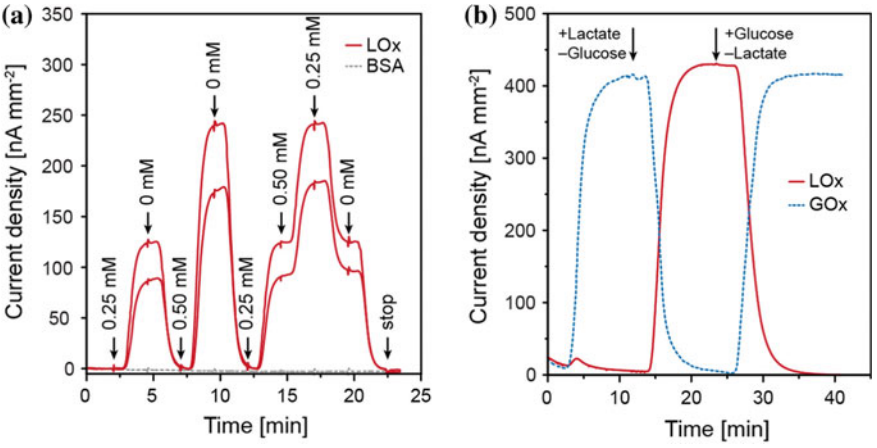

Fig. 8 Sensor on-chip response curves for lactate and glucose in PBS at 37 °C. **a** Lactate current signals recorded from two hanging drops in parallel. Electrodes were functionalized with lactate oxidase and BSA (blank electrode) in each of the two drops. Different concentrations of lactate were sequentially perfused. **b** On- chip lactate and glucose signals simultaneously recorded in PBS under an alternating analyte flow of glucose and lactate. Adapted from [39]

4 Real-Time Online Analyte Recording

4.1 Cell Culture and Microtissue Production

All cell-based experiments were carried out using the fluorescent human colon carcinoma cell line HCT116 eGFP. The cells were cultured in RPMI 1640 growth medium. Prior to an experiment, cells were harvested from the culture flasks for microtissue fabrication. The cell suspension was diluted with fresh medium containing all supplements. Cell concentration was adjusted with due regard to the experimental requirements and desired microtissue sizes.

GravityPLUS plates from InSphero AG, Switzerland, were used to form and grow microtissues from HCT116 eGFP cell suspensions inside hanging drops. After 3 days of incubation in the incubator, the microtissues were transferred to the GravityTRAP plate (InSphero) for maintenance and media exchange every 3 days.

4.2 Measurement of Analyte Secretion

Glucose and lactate biosensors were calibrated to determine the specific sensitivity per area (nA $mmol^{-1}$ L mm^{-2}) of each electrode. During the experiments, the current density (nA mm^{-2}) was constantly measured at a 10 Hz sampling rate. The corresponding analyte concentration was then calculated according to the previously determined sensitivity of the respective electrodes. This procedure enabled to continuously monitor the analyte concentration (mmol L^{-1}) in the hanging drops over time.

Continuous measurements, while perfusion was periodically switched on or off, were carried out, and the concentration change in the 10 µl hanging-drop compartment was recorded in real time (mmol L^{-1} h^{-1}). Secretion rates (mmol h^{-1}) were finally obtained by taking the volume of 10 µl into account.

A typical characteristic of cancerous tissue is an enhanced glucose uptake rate due to an increased glycolysis metabolism, through which pyruvate is fermented to lactate under aerobic conditions [19]. The performance of the device was assessed by measuring the metabolism of HCT116 eGFP cancer microtissues. Glucose uptake and lactate secretion were recorded in real time in the microfluidic hanging-drop network using the two developed biosensors.

Figure 9a presents measurements of lactate that was secreted from an HCT116 eGFP microtissue (480 µm in diameter) inserted in one of the sensor drops. The measurement was carried out in PBS, supplemented with 10 mM glucose, while perfusion was stopped. After the perfusion had been stopped, the lactate signal increased reproducibly to 73.8 ± 4.4 µmol l^{-1} as a result of lactate accumulation in the drop and then decreased again during the washing phase, when the drop liquid volume was exchanged with fresh PBS at a flow rate of 5 µl min^{-1}. A lactate

secretion rate of 2.21 nmol h^{-1} was calculated. This value is comparable to lactate secretion rates of growing HCT116 microtissues found in the literature [55]. As a negative control, the microtissue was removed from the hanging drop after four perfusion cycles. No lactate was detected after removal, which confirmed the microtissue being the source of the lactate. Further, no signal that may originate from other electro-active species was recorded on the blank electrode. A three-point calibration was performed prior to microtissue loading and after the experiment to calculate lactate concentrations.

Figure 9b shows in situ real-time measurements of glucose consumption and simultaneous lactate production of four HCT116 eGFP microtissues of similar size (274 ± 9 µm), which were inserted in pairs into two sensing drops. One drop comprised a glucose sensor and a blank BSA electrode for glucose detection. In the other drop, the electrodes were functionalized as lactate sensor and blank BSA. The measurement was carried out by switching between PBS and glucose-supplemented PBS solution (0.5 mM) using an on-off-perfusion protocol and a flow rate of 5 µl min^{-1}. After microtissue insertion and the infusion of the glucose solution (clearly visible through the steep glucose signal increase) the microtissues were cultured for 60 min without flow. The glucose signal decreased from its initial value of 500 µM. The consumption rate was calculated to 2.57 nmol h^{-1} for two microtissues. At the same time, lactate was secreted at a rate of 2.40 nmol h^{-1}. Comparable values for lactate secretion [55] and glucose consumption [3, 55] were found in the literature. The blank BSA working electrodes showed little cross talk. This cross-talk signal originates from hydrogen peroxide diffusion in the same

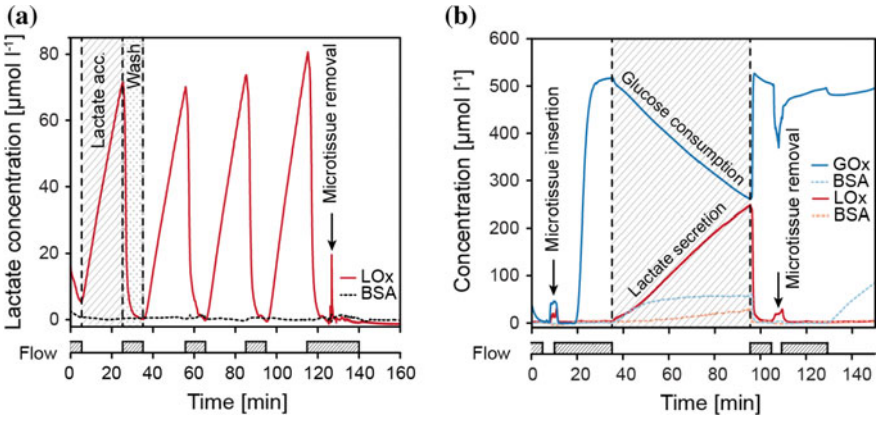

Fig. 9 Measuring the metabolism of human colon cancer microtissues (HCT116 eGFP) in the hanging-drop chip. The microtissues are cultured in glucose-enriched PBS at 37 °C. The measurements were carried out during an on–off medium perfusion protocol. **a** Lactate secretion was directly measured from one microtissue. **b** Real-time and simultaneous measurement of the glucose consumption and lactate secretion of cancer microtissues. Adapted from [39]

hanging-drop. The liquid was exchanged after 1 h restoring the initial sensor signal values for both sensor types. Microtissues were then removed from both sensing-drop sites. Perfusion was stopped again, and the conducted measurements confirmed that the recorded analyte transients indeed originated from the metabolism of the microtissues.

5 Conclusion

The modular approach of the analytical platform preserves all advantages of the hanging-drop network technology, including the adhesion-free liquid–air interface for spheroid cultures, a precise control of the liquid flow, bubble-free operation, inherent gas exchange, and full continuous access to the fluidic network, which enables loading and harvesting of liquid samples and spheroids for downstream analysis. Decoupling of the sensor unit from the microfluidic chip substantially reduces fabrication, assembly, and operation complexity of the integrated multi-functional platform. Critical procedures, such as biosensor functionalization and calibration, can be performed independently off-chip. Biosensors can, for example, be prepared, stored and plugged in just before use, when the microtissue structures are ready for the experiments. The developed functionalization procedure is simple, and its reproducibility has been improved through implementation of SU-8 electrode rims that support drop deposition.

The technological approach is highly versatile. Different versions of the microfluidic chip were fabricated, in which the biosensor modules could be plugged in at different locations in the hanging-drop network. The approach can be applied to more complex and larger hanging-drop networks including different spheroid types in multi-tissue configurations. Further, the readout capability of the system can be easily expanded through integration of additional plug-ins that comprise more and/or tissue-specific sensor types. The platform is very flexible in how sensors and hanging drops hosting the microtissues can be arranged.

Despite the fact that the presented approach allows for continuous sensor operation at sufficient sensitivity for approximately 1 day, biosensors always face the challenge of extended lifetime and good measurement reproducibility. We tried to address this challenge by using the plug-in approach: Sensors with satisfactory characteristics can be selected, pre- and post-calibration can be performed off-chip or by using an automated on-chip perfusion protocol during longer experiments.

Lactate and glucose metabolism of individual GFP-induced human colon carcinoma microtissues could be measured in situ inside a small, 10 µl volume by an automated perfusion setup so that any disturbance and influence of external effects could be effectively excluded. The obtained data provided real-time information in the time range of minutes on the metabolic state of the microtissues under different culture conditions.

Acknowledgements This work was financially supported by FP7 of the EU through the projects "Body on a chip", ICT-FET-296257 and the ERC Advanced Grant "NeuroCMOS" (contract 267351) as well as by an individual Ambizione Grant 142440 of the Swiss National Science Foundation for Olivier Frey.

References

1. Arquint P, Koudelka-Hep M, van der Schoot BH et al (1994) Micromachined analyzers on a silicon chip. Clin Chem 40:1805–1809
2. Asthana A, Kisaalita WS (2012) Microtissue size and hypoxia in HTS with 3D cultures. Drug Discov Today 17:810–817. https://doi.org/10.1016/j.drudis.2012.03.004
3. Aykin-Burns N, Ahmad IM, Zhu Y et al (2009) Increased levels of superoxide and H2O2 mediate the differential susceptibility of cancer cells versus normal cells to glucose deprivation. Biochem J 418:29–37. https://doi.org/10.1042/BJ20081258
4. Baharvand H, Hashemi SM, Kazemi Ashtiani S, Farrokhi A (2006) Differentiation of human embryonic stem cells into hepatocytes in 2D and 3D culture systems in vitro. Int J Dev Biol 50:645–652. https://doi.org/10.1387/ijdb.052072hb
5. Balcells M, Fernández Suárez M, Vázquez M, Edelman ER (2005) Cells in fluidic environments are sensitive to flow frequency. J Cell Physiol 204:329–335. https://doi.org/10.1002/jcp.20281
6. Beauchamp P, Moritz W, Kelm JM et al (2015) Development and characterization of a scaffold-free 3D spheroid model of induced pluripotent stem cell-derived human cardiomyocytes. Tissue Eng Part C Methods 21:852–861. https://doi.org/10.1089/ten.TEC.2014.0376
7. Boero C, Olivo J, De Micheli G, Carrara S (2012) New approaches for carbon nanotubes-based biosensors and their application to cell culture monitoring. IEEE Trans Biomed Circuits Syst 6:479–485. https://doi.org/10.1109/TBCAS.2012.2220137
8. Breslin S, O'Driscoll L (2013) Three-dimensional cell culture: the missing link in drug discovery. Drug Discov Today 18:240–249. https://doi.org/10.1016/j.drudis.2012.10.003
9. Brischwein M, Motrescu ER, Cabala E et al (2003) Functional cellular assays with multiparametric silicon sensor chips. Lab Chip 3:234–240. https://doi.org/10.1039/b308888j
10. Ciobanu M, Taylor DE, Wilburn JP, Cliffel DE (2008) Glucose and lactate biosensors for scanning electrochemical microscopy imaging of single live cells. Anal Chem 80:2717–2727. https://doi.org/10.1021/ac7021184
11. Dempsey E, Diamond D, Smyth MR et al (1997) Design and development of a miniaturised total chemical analysis system for on-line lactate and glucose monitoring in biological samples. Anal Chim Acta 346:341–349. https://doi.org/10.1016/S0003-2670(97)90075-1
12. Dittrich PS, Manz A (2006) Lab-on-a-chip: microfluidics in drug discovery. Nat Rev Drug Discov 5:210–218. https://doi.org/10.1038/nrd1985
13. Eklund SE, Taylor D, Kozlov E et al (2004) A microphysiometer for simultaneous measurement of changes in extracellular glucose, lactate, oxygen, and acidification rate. Anal Chem 76:519–527. https://doi.org/10.1021/ac034641z
14. El-Ali J, Sorger PK, Jensen KF (2006) Cells on chips. Nature 442:403–411. https://doi.org/10.1038/nature05063
15. Esch MB, Prot J-M, Wang YI et al (2015) Multi-cellular 3D human primary liver cell culture elevates metabolic activity under fluidic flow. Lab Chip 15:2269–2277. https://doi.org/10.1039/c5lc00237k

16. Esch MB, Smith AST, Prot J-M et al (2014) How multi-organ microdevices can help foster drug development. Adv Drug Deliv Rev 69–70:158–169. https://doi.org/10.1016/j.addr.2013.12.003
17. Frey O, Misun PM, Fluri DA et al (2014) Reconfigurable microfluidic hanging drop network for multi-tissue interaction and analysis. Nat Commun 5:4250. https://doi.org/10.1038/ncomms5250
18. Frey O, Talaei S, van der Wal PD et al (2010) Continuous-flow multi-analyte biosensor cartridge with controllable linear response range. Lab Chip 10:2226–2234. https://doi.org/10.1039/c004851h
19. Gatenby RA, Gillies RJ (2004) Why do cancers have high aerobic glycolysis? Nat Rev Cancer 4:891–899. https://doi.org/10.1038/nrc1478
20. Ges IA, Baudenbacher F (2010) Enzyme electrodes to monitor glucose consumption of single cardiac myocytes in sub-nanoliter volumes. Biosens Bioelectron 25:1019–1024. https://doi.org/10.1016/j.bios.2009.09.018
21. Ges IA, Baudenbacher F (2010) Enzyme-coated microelectrodes to monitor lactate production in a nanoliter microfluidic cell culture device. Biosens Bioelectron 26:828–833. https://doi.org/10.1016/j.bios.2010.05.030
22. Grieshaber D, MacKenzie R, Vörös J, Reimhult E (2008) Electrochemical biosensors—sensor principles and architectures. Sensors 8:1400–1458. https://doi.org/10.3390/s8031400
23. Griffith LG, Swartz MA (2006) Capturing complex 3D tissue physiology in vitro. Nat Rev Mol Cell Biol 7:211–224. https://doi.org/10.1038/nrm1858
24. Hafner F (2000) Cytosensor Microphysiometer: technology and recent applications. Biosens Bioelectron 15:149–158. https://doi.org/10.1016/S0956-5663(00)00069-5
25. Hirschhaeuser F, Menne H, Dittfeld C et al (2010) Multicellular tumor spheroids: an underestimated tool is catching up again. J Biotechnol 148:3–15. https://doi.org/10.1016/j.jbiotec.2010.01.012
26. Huh D, Matthews BD, Mammoto A et al (2010) Reconstituting organ-level lung functions on a chip. Science 328:1662–1668. https://doi.org/10.1126/science.1188302
27. Huh D, Torisawa Y, Hamilton GA et al (2012) Microengineered physiological biomimicry: organs-on-chips. Lab Chip 12:2156–2164. https://doi.org/10.1039/c2lc40089h
28. Justice BA, Badr NA, Felder RA (2009) 3D cell culture opens new dimensions in cell-based assays. Drug Discov Today 14:102–107. https://doi.org/10.1016/j.drudis.2008.11.006
29. Kelm JM, Timmins NE, Brown CJ et al (2003) Method for generation of homogeneous multicellular tumor spheroids applicable to a wide variety of cell types. Biotechnol Bioeng 83:173–180. https://doi.org/10.1002/bit.10655
30. Kim J-Y, Fluri DA, Marchan R et al (2015) 3D spherical microtissues and microfluidic technology for multi-tissue experiments and analysis. J Biotechnol 205:24–35. https://doi.org/10.1016/j.jbiotec.2015.01.003
31. Knight E, Przyborski S (2014) Advances in 3D cell culture technologies enabling tissue-like structures to be created in vitro. J Anat. https://doi.org/10.1111/joa.12257
32. Kovarik ML, Gach PC, Ornoff DM et al (2012) Micro total analysis systems for cell biology and biochemical assays. Anal Chem 84:516–540. https://doi.org/10.1021/ac202611x
33. Lee J, Cuddihy MJ, Kotov NA (2008) Three-dimensional cell culture matrices: state of the art. Tissue Eng Part B Rev 14:61–86. https://doi.org/10.1089/teb.2007.0150
34. Link H, Fuhrer T, Gerosa L et al (2015) Real-time metabolome profiling of the metabolic switch between starvation and growth. Nat Methods 12:1091–1097. https://doi.org/10.1038/nmeth.3584
35. Lu H, Koo LY, Wang WM et al (2004) Microfluidic shear devices for quantitative analysis of cell adhesion. Anal Chem 76:5257–5264. https://doi.org/10.1021/ac049837t

36. Maschmeyer I, Lorenz AK, Schimek K et al (2015) A four-organ-chip for interconnected long-term co-culture of human intestine, liver, skin and kidney equivalents. Lab Chip 15:2688–2699. https://doi.org/10.1039/c5lc00392j
37. McKenzie JR, Palubinsky AM, Brown JE et al (2012) Metabolic multianalyte microphysiometry reveals extracellular acidosis is an essential mediator of neuronal preconditioning. ACS Chem Neurosci 3:510–518. https://doi.org/10.1021/cn300003r
38. Messner S, Agarkova I, Moritz W, Kelm JM (2013) Multi-cell type human liver microtissues for hepatotoxicity testing. Arch Toxicol 87:209–213. https://doi.org/10.1007/s00204-012-0968-2
39. Misun PM, Rothe J, Schmid YRF et al (2016) Multi-analyte biosensor interface for real-time monitoring of 3D microtissue spheroids in hanging-drop networks. Microsystems Nanoeng 2:16022. https://doi.org/10.1038/micronano.2016.22
40. Moser I, Jobst G, Urban GA (2002) Biosensor arrays for simultaneous measurement of glucose, lactate, glutamate, and glutamine. Biosens Bioelectron 17:297–302
41. Nge PN, Rogers CI, Woolley AT (2013) Advances in microfluidic materials, functions, integration, and applications. Chem Rev 113:2550–2583. https://doi.org/10.1021/cr300337x
42. Pampaloni F, Reynaud EG, Stelzer EHK (2007) The third dimension bridges the gap between cell culture and live tissue. Nat Rev Mol Cell Biol 8:839–845. https://doi.org/10.1038/nrm2236
43. Perdomo J, Hinkers H, Sundermeier C et al (2000) Miniaturized real-time monitoring system for L-lactate and glucose using microfabricated multi-enzyme sensors. Biosens Bioelectron 15:515–522
44. Pitta Bauermann L, Schuhmann W, Schulte A (2004) An advanced biological scanning electrochemical microscope (Bio-SECM) for studying individual living cells. Phys Chem Chem Phys 6:4003. https://doi.org/10.1039/b405233a
45. Polini A, Prodanov L, Bhise NS et al (2014) Organs-on-a-chip: a new tool for drug discovery. Expert Opin Drug Discov 9:335–352. https://doi.org/10.1517/17460441.2014.886562
46. Powers MJ, Janigian DM, Wack KE et al (2002) Functional behavior of primary rat liver cells in a three-dimensional perfused microarray bioreactor. Tissue Eng 8:499–513. https://doi.org/10.1089/107632702760184745
47. Rimann M, Laternser S, Gvozdenovic A et al (2014) An in vitro osteosarcoma 3D microtissue model for drug development. J Biotechnol 189:129–135. https://doi.org/10.1016/j.jbiotec.2014.09.005
48. Rothe J, Frey O, Stettler A et al (2014) Fully integrated CMOS microsystem for electrochemical measurements on 32 × 32 working electrodes at 90 frames per second. Anal Chem 86:6425–6432. https://doi.org/10.1021/ac500862v
49. Satoh W, Hosono H, Yokomaku H et al (2008) Integrated electrochemical analysis system with microfluidic and sensing functions. Sensors 8:1111–1127. https://doi.org/10.3390/s8021111
50. Sonntag F, Schilling N, Mader K et al (2010) Design and prototyping of a chip-based multi-micro-organoid culture system for substance testing, predictive to human (substance) exposure. J Biotechnol 148:70–75. https://doi.org/10.1016/j.jbiotec.2010.02.001
51. Stucki AO, Stucki JD, Hall SRR et al (2015) A lung-on-a-chip array with an integrated bio-inspired respiration mechanism. Lab Chip 15:1302–1310. https://doi.org/10.1039/c4lc01252f
52. Sung JH, Kam C, Shuler ML (2010) A microfluidic device for a pharmacokinetic-pharmacodynamic (PK-PD) model on a chip. Lab Chip 10:446–455. https://doi.org/10.1039/b917763a

53. Talaei S, van der Wal PD, Ahmed S et al (2015) Enzyme SU-8 microreactors: simple tools for cell-culture monitoring. Microfluid Nanofluidics 19:351–361. https://doi.org/10.1007/s10404-015-1562-8
54. Tibbitt MW, Anseth KS (2009) Hydrogels as extracellular matrix mimics for 3D cell culture. Biotechnol Bioeng 103:655–663. https://doi.org/10.1002/bit.22361
55. Timmins NE, Dietmair S, Nielsen LK (2004) Hanging-drop multicellular spheroids as a model of tumour angiogenesis. Angiogenesis 7:97–103. https://doi.org/10.1007/s10456-004-8911-7
56. Tung Y-C, Hsiao AY, Allen SG et al (2011) High-throughput 3D spheroid culture and drug testing using a 384 hanging drop array. Analyst 136:473–478. https://doi.org/10.1039/c0an00609b
57. Van der Meer AD, Poot AA, Feijen J, Vermes I (2010) Analyzing shear stress-induced alignment of actin filaments in endothelial cells with a microfluidic assay. Biomicrofluidics 4:11103. https://doi.org/10.1063/1.3366720
58. Van Midwoud PM, Merema MT, Verpoorte E, Groothuis GMM (2010) A microfluidic approach for in vitro assessment of interorgan interactions in drug metabolism using intestinal and liver slices. Lab Chip 10:2778–2786. https://doi.org/10.1039/c0lc00043d
59. Weltin A, Slotwinski K, Kieninger J et al (2014) Cell culture monitoring for drug screening and cancer research: a transparent, microfluidic, multi-sensor microsystem. Lab Chip 14:138–146. https://doi.org/10.1039/c3lc50759a
60. Young EWK, Beebe DJ (2010) Fundamentals of microfluidic cell culture in controlled microenvironments. Chem Soc Rev 39:1036–1048. https://doi.org/10.1039/b909900j
61. Zhang C, Zhao Z, Abdul Rahim NA et al (2009) Towards a human-on-chip: culturing multiple cell types on a chip with compartmentalized microenvironments. Lab Chip 9:3185–3192. https://doi.org/10.1039/b915147h